Molecular Crystals and Liquid Crystals

ISSN: 1542-1406 (Print) 1563-5287 (Online) Journal homepage: http://www.tandfonline.com/loi/gmcl20

Crystal structure, spectroscopic investigations, and density functional studies of (Z)-2-(1H-imidazol-1-yl)-1-(3-methyl-3-mesitylcyclobutyl)ethanone oxime

H. Saraçoğlu & A. Cukurovali

To cite this article: H. Saraçoğlu & A. Cukurovali (2016) Crystal structure, spectroscopic investigations, and density functional studies of (Z)-2-(1H-imidazol-1-yl)-1-(3-methyl-3-mesitylcyclobutyl)ethanone oxime, Molecular Crystals and Liquid Crystals, 625:1, 173-185, DOI: 10.1080/15421406.2015.1069443

To link to this article: http://dx.doi.org/10.1080/15421406.2015.1069443

Published online: 19 Feb 2016.

MOL. CRYST. LIQ. CRYST.
2016, VOL. 625, 173–185
http://dx.doi.org/10.1080/15421406.2015.1069443

Taylor & Francis
Taylor & Francis Group

Crystal structure, spectroscopic investigations, and density functional studies of (Z)-2-(1*H*-imidazol-1-yl)-1-(3-methyl-3-mesitylcyclobutyl)ethanone oxime

H. Saraçoğlu[a] and A. Cukurovali[b]

[a]Department of Middle Education, Educational Faculty, Ondokuz Mayis University, Kurupelit, Samsun, Turkey; [b]Department of Chemistry, Faculty of Sciences, Firat University, Elazig, Turkey

ABSTRACT

The title molecule, (Z)-2-(1H-imidazol-1-yl)-1-(3-methyl-3-mesitylcyclobutyl)ethanone oxime (C_{19} H_{25} N_3 O), was prepared and characterized by ^{1}H-Nuclear magnetic resonance (NMR), ^{13}C-NMR, infrared spectroscopic methods, and X-ray single-crystal determination. The compound crystallizes in the orthorhombic space group P c c n with $a = 31.4660(17)$ Å, $b = 11.2140(7)$ Å, and $c = 10.0710(8)$ Å. In addition to molecular geometry from X-ray determination, vibrational frequencies and gauge, including atomic orbital, ^{1}H- and ^{13}C-NMR chemical shift values of the title compound in the ground state, were calculated using the density functional method with the 6-31G(d) basis set. The calculated results show that the optimized geometries can well reproduce the crystal structure. Besides, the theoretical vibrational frequencies and chemical shift values show good agreement with experimental values. The predicted nonlinear optical properties of the title compound are greater than those of urea. Density functional theory calculations of molecular electrostatic potentials, frontier molecular orbitals, and thermodynamic properties of the title compound were carried out at the B3LYP/6-31G(d) level of theory.

KEYWORDS

Computational chemistry; imidazoles; NMR spectroscopy; nonlinear optical properties; oximes

Introduction

The imidazole scaffold is forecasted to be a good pharmacophore and represents an important synthetic precursor in new drug discovery [1–3]. These scaffolds play very important role as mediators in synthetic reactions, primarily for preparing functionalized materials [4–6]. Heterocyclic imidazole derivatives have also attracted considerable attention exhibiting various biological applications as anti-HIV [7], anticonvulsant [8], antitubercular [9], and FTase and MAP kinase p38 inhibitory activities [10, 11]. In particular, nitroimidazoles exhibit interesting therapeutic applications as anaerobic antibacterial [1] and anti-protozoal agents [12], radio sensitizers [13, 14], and hypoxia detecting chemo-sensitizers. Not only the most popular anticancer drugs carboplatin and lobaplatin but enloplatin, mibaplatin, sebriplatin, and zenitplatin are also cyclobutane derivatives and are used as effective anticancer drugs [15]. Oxime compounds are used as anti-chemical warfare agents such as atropine or atropine sulfate, where oximes reactivate phosphonylated AChE through a nucleophilic reaction [16]. In

CONTACT H. Saraçoğlu hanifesa@omu.edu.tr Department of Middle Education, Educational Faculty, Ondokuz Mayis University, 55139 Kurupelit, Samsun, Turkey.
Color versions of one or more of the figures in the article can be found online at www.tandfonline.com/gmcl.

the light of the above-given effects, the compounds containing cyclobutane, oxime, and imidazole functionalities in one molecule have seen to be important.

In this work, we present the results of a detailed investigations of (Z)-2-(1H-imidazol-1-yl)-1-(3-methyl-3-mesitylcyclobutyl)ethanone oxime by using single crystal X-ray and quantum chemical methods. The vibrational assignments of the title compound in the ground state have been calculated by using the density functional theory (DFT) (B3LYP) method with 6-31G(d) basis set. The structural geometry, molecular electrostatic potential (MEP), and frontier molecular orbitals (FMO) of the title compound were studied at the B3LYP/6-31G(d) level. Nonlinear optical (NLO) properties of the title compound were also investigated. A comparison of the experimental and theoretical spectra can be very useful in making correct assignments and understanding the basic chemical shift–molecular structure relationship. Hence, these calculations are valuable for providing insight into molecular properties of imidazole- and oxime-based compounds.

Experimental

Synthesis of the title compound

To a solution of 1-methyl-1-mesityl-3-(2-chloro-1-oxoethyl) cyclobutane (α–haloketone) (2.6479 g, 10 mmol) in 20 mL of dry dimethylformamide (DMF), a solution of imidazole (0.6808 g, 10 mmol) in 10 mL of dry DMF was added drop-wise in the presence of K_2CO_3 (10 mmol), and the mixture was stirred overnight. End of the reaction was determined by monitoring the course of the reaction with infrared (IR) spectroscopy. Subsequently, a solution of hydroxylamine hydrochloride (0.6949 g, 10 mmol) in 20 mL of DMF was added drop-wise and refluxed for 2 h (IR). The solution was cooled to room temperature and poured into water, and white precipitate separated by suction was washed with water for several times and dried in air. Suitable single crystals for determination of crystal structure were obtained by slow evaporation of its ethanol solution. The synthesis of the title compound is shown in Scheme 1. Silky brilliant crystals: Overall yield: 72.6%; m.p.: 477 K (EtOH).

Crystal structure determination

The data collection was performed at 296 K on a Stoe-IPDS-2 diffractometer equipped with a graphite monochromated Mo-K_α radiation ($\lambda = 0.71073$ Å). The structure was solved by direct methods using SHELXS-97 and refined by a full-matrix, least-squares procedure using the program SHELXL-97 [17]. All non-hydrogen atoms were easily found from different Fourier maps and refined anisotropically. All hydrogen atoms were included using a riding model and refined isotropically with CH = 0.93 (for mesityl and imidazole groups), CH =

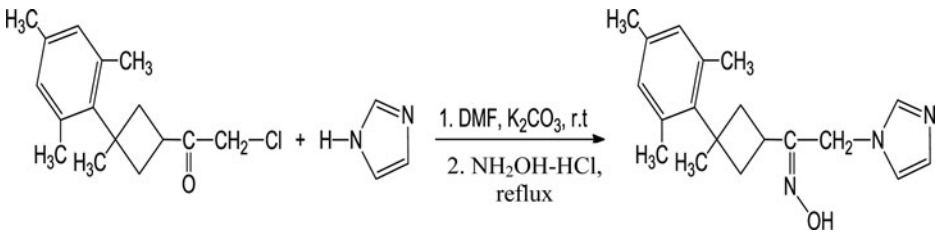

Scheme 1. Reaction sequence for the synthesis of the title compound.

Table 1. Crystallographic data for the title compound.

Empirical formula	$C_{19}\,H_{25}\,N_3\,O$
Molecular weight	311.42
Temperature, *T* (K)	296
Wavelength (Å)	0.71073
Crystal system	Orthorhombic
Space group	P c c n
a (Å)	31.4660(17)
b (Å)	11.2140(7)
c (Å)	10.0710(8)
Volume, *V* (Å^3)	3553.7(4)
Z	8
Calculated density (g/cm^3)	1.164
μ/mm^{-1}	0.073
F(000)	1344
Crystal size(mm)	0.315 × 0.274 × 0.129
Θ range(°)	27.74/3.34
Index range (h, k, l)	−40/22, −7/14, −11/12
Reflections collected	9437
Independent reflections (R_{int})	3600 (0.067)
Observed reflections[I > 2σ(I)]	1364
Data/parameters	3600/209
Goodness-of-fit on F^2	1.02
Final *R* indices [I > 2σ(I)]	0.086
wR indices [I > 2σ(I)]	0.186
Largest diff. peak and hole (e.Å^{-3})	0.24 and −0.18

0.98, CH_2 = 0.97, CH_3 = 0.96, and OH = 0.82 Å. $U_{iso}(H) = 1.2U_{eq}$. Details of the data collection conditions and the parameters of the refinement process are given in Table 1.

Theoretical methods

The molecular structure of the title compound in the ground state (in vacuo) was optimized by the B3LYP method with 6-31G(d) basis set. For modeling, the initial guess of the title compound was first obtained from X-ray coordinates. Then vibrational frequencies for optimized molecular structure were calculated and scaled by 0.9833 [18]. The geometry of the title compound, together with that of tetramethylsilane (TMS), was fully optimized. ^{1}H- and ^{13}C-NMR chemical shifts were calculated within the gauge, including atomic orbital (GIAO) approach [19, 20] applying the B3LYP method with 6-31G(d) basis set. All the calculations were performed by using Gauss-view molecular visualization program [21] and Gaussian 03 program package [22] on personal computer without specifying any symmetry for the title molecule.

To investigate the reactive sites of the title compound, the MEP was evaluated using the B3LYP/6-31G(d) method. MEP, *V*(r), at a given point r(x, y, z) in the vicinity of the molecule is defined in terms of the interaction energy between the electrical charge generated by the molecule's electrons and nuclei and a positive test charge (a proton) located at r. For the system studied, the *V*(r) values were calculated as described previously using the equation given in [23],

$$V\,(\mathrm{r}) = \sum \frac{Z_A}{|R_A - \mathrm{r}|} - \int \frac{\rho\,(r')}{|r' - \mathrm{r}|} d^3 r', \tag{1}$$

where Z_A is the charge of nucleus A, located at R_A, $\rho\,(r')$ is the electronic density function of the molecule, and r' is the dummy integration variable. The linear polarizability and the first

hyperpolarizability properties of the title compound were obtained by molecular polarizabilities based on theoretical calculations.

Results and discussion

Description of crystal structure

The crystal structure of the title compound is orthorhombic and space group P c c n with eight molecules in the unit cell. The molecular structure of the title compound as shown in Fig. 1 is not planar, but phenyl and imidazole rings are planar individually. The asymmetric unit in the crystal structure contains only one molecule.

Molecule $C_{19}H_{25}N_3O$ contains imidazole, mesityl, and cyclobutane rings. The imidazole and mesityl rings are planar with maximum deviations of 0.0056(26) Å and −0.0292(28) Å, respectively. The dihedral angles between the cyclobutane plane A (C10–C13), the imidazole plane B (N2/N3/C17–C19), and the mesityl plane C (C1–C6) are 79.51(20)° (A/B), 37.60(26)° (A/C), and 68.19 (15)° (B/C). Rings A and B are nearly perpendicular to one another.

In the imidazole ring, the N2−C17 and C17−N3 bond lengths (Table 2) are in agreement with the literature values [24,25]. The C18–C19 bond distance of 1.334(7) Å is also in agreement with the value of C=C double-bond character [26].

The steric interaction between the substituent groups on the cyclobutane ring means that this ring derivates significantly from planarity. In the cyclobutane ring, the C11/C12/C13 plane forms a dihedral angle of 26.78(41)° with the C13/C10/C11 plane. A survey of the geometry of cyclobutanes shows the average pucker to be 26.8(2)° [27], 27.03(3)° and 28.16(3)° [28], and 25.74(15)° [29] in acyclic-substituted cyclobutane rings, and the present value is in agreement with the previous reports.

The oxime moiety in (I) has an E configuration, with a C12−C15−N1−O torsion angle of –175.4(3)°. In this conformation, atom O of the oxime group behaves as a donor, resulting in the formation of O−H …N hydrogen bonds, which link two molecules related by a C_4^4 (16) chain running parallel to the $[0\bar{1}0]$ direction (Fig. 2). There is also an intramolecular C16−H16B …O hydrogen bond forming S(5) motif [30]. These intermolecular hydrogen bonds are highly effective in forming polymeric chains, thereby stabilizing the crystal structure (Table 3). Besides these, hydrogen bonds have $\pi \ldots \pi$ interactions, which stabilize the title compound.

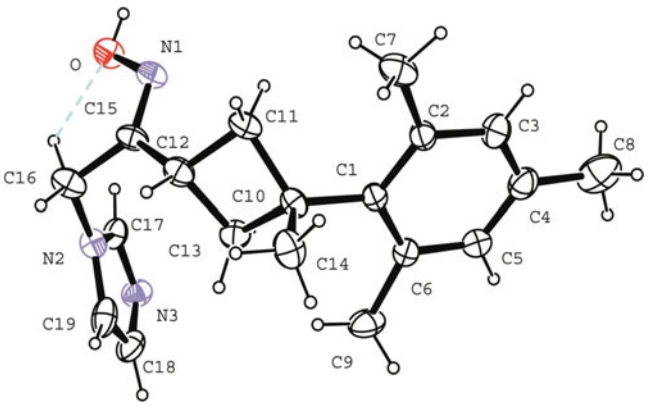

Figure 1. Ortep III diagram of the title compound. Displacement ellipsoids are drawn at the 30% probability level, and H atoms are shown as small spheres of arbitrary radii.

Table 2. Selected theoretical and experimental geometric parameters of the title compound.

	Experimental	B3LYP 6-31G(d)
Bond lengths (Å)		
O-N1	1.411(4)	1.412
N1-C15	1.262(5)	1.282
C15-C16	1.506(6)	1.522
C12-C15	1.495(6)	1.503
N2-C16	1.462(5)	1.463
N2-C17	1.350(5)	1.370
N2-C19	1.363(5)	1.383
C18-C19	1.334(7)	1.372
N3-C17	1.302(5)	1.317
N3-C18	1.358(6)	1.377
RMSE[a]		0.019
Max. difference[a]		0.038
Bond Angles (°)		
O-N1-C15	113.3(4)	112.59
N1-C15-C12	118.0(4)	117.77
N1-C15-C16	123.8(4)	123.60
C15-C16-N2	111.7(3)	112.80
C12-C15-C16	118.1(5)	118.63
C16-N2-C19	129.0(5)	126.86
C16-N2-C17	125.7(4)	126.69
C15-C12-C11	120.5(4)	120.09
RMSE[a]		0.988
Max. difference[a]		2.140
Dihedral angles (°)		
C12-C15-N1-O	− 175.4(3)	177.96
N1-C15-C16-N2	− 100.2(5)	94.13
C12-C15-C16-N2	76.5(5)	–85.07
C15-C16-N2-C17	76.6(5)	–69.03
C13-C12-C15-N1	99.0(5)	–104.55
C11-C12-C15-N1	− 5.8(6)	0.74

[a]RMSE and maximum differences between bond lengths and bond angles computed by the theoretical method and those obtained from X-ray diffraction.

Optimized structure (I)

The molecular structure of the title compound ($C_{19}H_{25}N_3O$) in the ground state (in vacuo) is optimized by using the B3LYP/6-31G(d) method. Some selected geometric parameters are experimentally obtained and theoretically calculated by using the B3LYP/6-31G(d) method. As seen in Table 2, most of the calculated bond lengths and the bond angles are slightly different from the experimental ones. We noted that the experimental results belong to the solid phase and the theoretical calculations belong to the gaseous phase. In the solid state, the experimental results are related to molecular packing, but in the gas phase, the isolated molecules are considered in the theoretical calculations. The biggest difference in bond lengths between experimental and predicted values is found at the C18–C19 bond, with the difference being 0.038 Å for the B3LYP method, whereas the biggest difference for the bond angles is found as 2.140° at C16–N2–C19. Using the root mean square error (RMSE) for evaluation, RMSE values of bond lengths and angles are 0.019 Å and 0.988°, respectively. In addition, the dihedral angles between optimized counterparts of the title compound are calculated at 84.60° (A/B), 39.80° (A/C), and 59.57° (B/C) for DFT/6-31G(d). In spite of the differences observed, the calculated geometric parameters are, in general, in good agreement with the X-ray structure.

IR spectroscopy

Fourier transform infrared (FT-IR) spectrum was obtained in KBr discs using a Mattson 1000 FT-IR spectrometer, and is shown in Fig. 3. Harmonic vibrational frequencies of the title

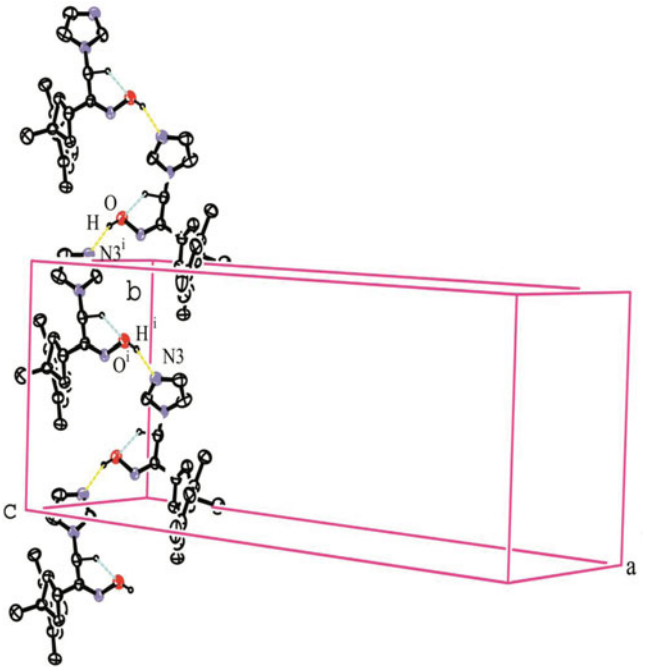

Figure 2. A diagram showing the O—H …N intermolecular hydrogen bonds in the title compound. Only H atoms involved in the hydrogen bonding interactions are shown. [Symmetry code: $-x, -\frac{1}{2}+ -\frac{1}{2}+y, z$]

compound were calculated by using the DFT method with the 6-31G(d) basis set, and the obtained frequencies were scaled by 0.9833 [18]. By using the Gauss–View molecular visualization program [21], the vibrational band assignments have been made. The calculated and experimental frequencies show differences. Two factors may be responsible for discrepancies between the experimental and the computed spectra of the investigated molecule. The first reason is that the experimental spectrum has been recorded for the compound in the solid state, while the computed spectra correspond to isolated molecule in the gas phase. The second reason is that the experimental values correspond to nonharmonic vibrations, while the calculated values are harmonic vibrations [31]. In order to facilitate assignment of observed peaks, we analyzed vibrational frequencies and compared our calculation of the title compound with their experimental results, and are shown in Table 4.

The free hydroxyl group absorbs strongly in the region 3700–3584 cm^{-1}, whereas the existence of intermolecular hydrogen bond formation can lower the O–H stretching frequency to the 3550–3200 cm^{-1} region with increase in intensity and breadth [32,33]. The experimental O–H stretching mode was observed at 3441 cm^{-1}, which has been calculated at 3698 cm^{-1} for B3LYP level. The aromatic structure shows the presence of C–H stretching vibrations in the region 2900–3150 cm^{-1}, which is the characteristic region for the ready identification of C–H

Table 3. Hydrogen bond geometries in crystal structure.

D–H···A (°)	D–H (Å)	H···A (Å)	D···A (Å)	D–H···A (°)
C16–H16B···O	0.97	2.27	2.660(6)	103
O–HO···N3^{i}	0.82	1.92	2.699(5)	158

Symmetry code: (i): $-x, -1/2 + y, 1/2 - z$.

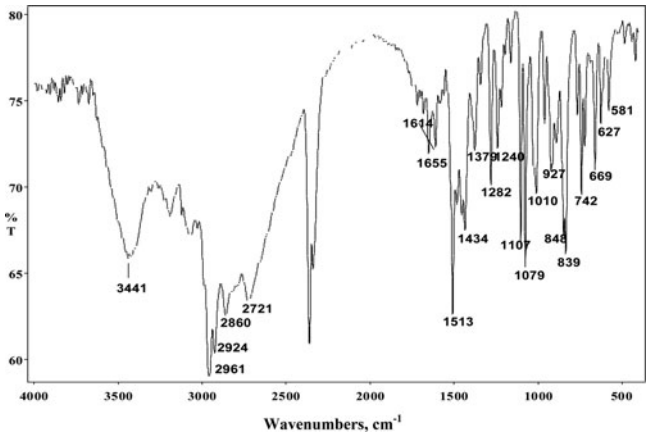

Figure 3. FT-IR spectrum of the title compound.

stretching vibrations [34]. In the present study, the symmetric and asymmetric C–H stretching vibrations of the title compound were calculated at 3116 cm^{-1} and 3112 cm^{-1} for B3LYP, respectively. The symmetric CH_2 stretching vibration is generally observed in the region of 2900–2800 cm^{-1} [35,36]. The band at 2860 cm^{-1} corresponds to the symmetric stretching CH_2 mode. This band has been calculated at 3032 cm^{-1} for B3LYP. The experimental C=N and C=C stretch bands were observed at 1655 cm^{-1} and 1513 cm^{-1}, which have been calculated with the DFT method at 1532 cm^{-1} and 1517 cm^{-1}. The other calculated vibrational frequencies can be seen in Table 4. As can be seen in Table 4, there is also a good agreement between experimental and theoretical vibration data of others.

Molecular electrostatic potential

The MEP is related to electronic density and is a very useful descriptor in understanding the sites of electrophilic attack and nucleophilic reactions as well as hydrogen bonding interactions [37–39]. The electrostatic potential $V(r)$ is also well suited for analyzing processes based on the "recognition" of one molecule by another, such as in drug–receptor and enzyme–substrate interactions because it is through their potentials that the two species first "see" each other [40,41]. Being a real physical property, $V(r)$ can be determined experimentally by diffraction or by computational methods [42].

Molecular electrostatic potential was calculated by using the B3LYP/6-31G(d) method. The red and blue regions of MEP represent negative and positive potentials, respectively. As can be seen in Fig. 4, this molecule has one possible site of electrophilic attack. The negative region is localized on the unprotonated nitrogen atom of imidazole ring, N3, with minimum value of −0.069 a.u. However, maximum positive region is localized on the hydrogen atom of oxime group, which can be considered as one possible site for nucleophilic attack, with a maximum value of 0.059 a.u. According to these calculated results, the MEP map shows that the negative potential site is on electronegative nitrogen atom and the positive potential sites are around hydrogen atoms.

The MEP is best suited for identifying sites for intra- and intermolecular interactions [43]. For the MEP surface in the title molecule, the negative region associated with N3 atom and also the positive region by the nearby HO atom are indicative of an intermolecular (N3···HO–O) hydrogen bonding.

Table 4. Comparison of the observed and calculated vibrational spectra of the title compound.

Assignments	Experimental	B3LYP 6-31G(d)
ν O-H	3441	3698
ν_s C-H (aromatic)		3116
ν_{as} C-H (aromatic)		3112
ν_{as} C-H_2		3103
ν_{as} C-H_2		3093
ν_{as} C-H_3		3078
ν_{as} C-H_3		3069
ν_{as} C-H_3		3065
ν_{as} C-H_3	2961	3063
ν_{as} C-H_3	2924	3055
ν_s C-H_2		3043
ν_{as} C-H_3		3042
ν_s C-H_2	2860	3032
ν_s C-H_3		3007
ν_s C-H_3		3006
ν_s C-H_3 + ν C-H		2994
ν_s C-H_3	2721	2989
ν C=N (imidazole)	1655	1532
α CH_3 + γ CH	1614	1520
ν C = C (imidazole)	1513	1517
α CH_3		1506
α CH_2	1434	1479
γ CH + γ CH_2	1379	1395
γ OH + γ CH	1282	1368
γ CH_2		1360
ν C = C (aromatic)		1300
ν C = C (imidazole)	1240	1295
ν C = C (imidazole)	1107	1240
γ CH_2 + γ OH	1010	1238
γ CH_2		1232
ν C-N (imidazole)		1127
α CH (aromatic)		1088
θ (aromatic) + β CH_3	927	1081
θ (imidazole)		1027
α CH_2	848	1012
ω CH_2	839	962
ω CH_2		938
γ CH_2		911
ω CH (aromatic)	742	860
ω CH (imidazole)	669	814
ω CH_2		717
δ CH (imidazole)	627	704
δ CH (imidazole)	581	666

Vibrational modes: ν, stretching; β, bending; α, scissoring; γ, rocking; ω, wagging; δ, twisting; θ, ring breathing; s, symmetric; as, asymmetric.

^{1}H- and ^{13}C-NMR spectra

GIAO ^{1}H- and ^{13}C chemical shift values (with respect to TMS) calculated by the B3LYP method with 6-31G(d) basis set were compared with the experimental ^{1}H and ^{13}C chemical shift values. The results are given in Table 5.

Since experimental ^{1}H chemical shift values were not available for individual hydrogen, we have presented the average values of CH_2 and CH_3 hydrogen atoms. The singlet observed at 2.93 ppm is assigned to H12 (C12) atoms, which have been calculated at 2.93 ppm for

Figure 4. Molecular electrostatic potential (MEP) map calculated at the B3LYP/6-31G(d) level.

Table 5. Theorical and experimental ^{13}C and ^{1}H isotropic chemical shifts (with respect to TMS all values are in ppm) for the title compound.

Atom	Experimental $CDCl_3$ (ppm)	Calculated chemical shift (ppm) B3LYP
C1	143.60	137.40
C2	134.94	129.38
C3	130.17	124.39
C4	134.65	128.21
C5	130.17	125.14
C6	134.94	129.47
C7	20.27	23.43
C8	21.28	21.38
C9	20.27	23.06
C10	40.53	43.81
C11	41.61	36.99
C12	31.61	37.01
C13	41.61	44.29
C14	23.69	24.60
C15	155.90	152.58
C16	47.59	42.04
C17	137.07	128.98
C18	128.79	121.76
C19	119.05	112.28
H3	6.77	6.62
H5	6.77	6.53
H7[a]	2.18	2.04
H8[a]	2.24	2.05
H9[a]	2.18	1.84
H11[a]	2.25–2.29	2.17
H12	2.93	2.93
H13[a]	2.49–2.56	2.57
H14[a]	1.49	1.43
H16[a]	4.87	4.41
H17	7.56	7.46
H18	6.96	6.72
H19	7.13	6.31
HO	10.65	6.33

[a]Average.

B3LYP level. The -CH_2- signals of the cyclobutane are observed at 2.25–2.29 ppm and 2.49–2.56 ppm, respectively. The aromatic-H and imidazole–H atoms were observed to be 6.77 (H3, H5) ppm and 6.96–7.56 (H17, H18, H19) ppm, respectively. The O–H hydrogen in the oxime group was observed at 10.65 ppm. The oxime group in the formation of both intermolecular and intramolecular hydrogen bonds causes the deviation of chemical shift value and so H atom contributes to the downfield resonance. ^{13}C-NMR spectra of the imidazole ring show the signals at 119.05–137.07 ppm due to C atoms. These signals have been calculated as 112.28–128.98 ppm for B3LYP level. Table 5 shows the other calculated chemical shift values. As can be seen in Table 5, calculated ^{1}H and ^{13}C chemical shift values of the title compound are generally in agreement with the experimental ^{1}H and ^{13}C shift data.

Frontier molecular orbital analysis

The frontier molecular orbitals play an important role in electric and optical properties as well as in UV-Vis spectra and chemical reactions [44]. The distributions and energy levels of the highest occupied molecular orbitals (HOMO)-1 and HOMO, and that of the lowest unoccupied molecular orbitals (LUMO) and LUMO+1 computed at the B3LYP/6-31G(d) method for the title compound are shown in Fig. 5.

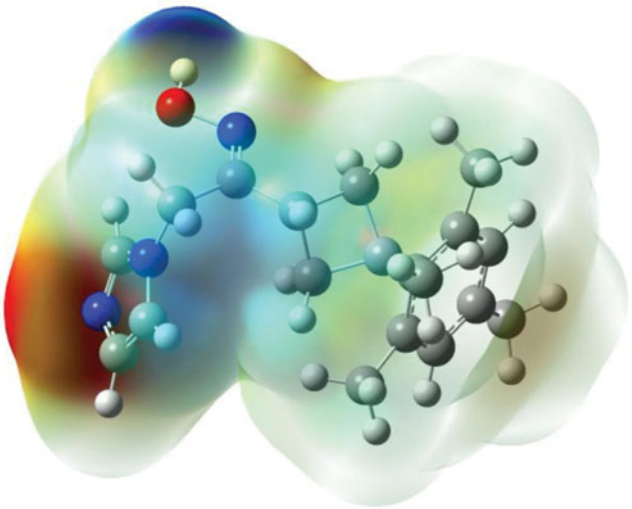

Figure 5. Plots of frontier orbitals of the title compound.

As seen in Fig. 5, the HOMO orbital is mainly localized on the imidazole ring. However, the LUMO+1 orbital is localized on the mesityl ring and partially localized on the cyclobutane ring of the title molecule. The HOMO-1 orbital is also localized on the mesityl and cyclobutane rings. LUMO orbital is delocalized on the title molecule except for mesityl ring. Both HOMO-1 and HOMO orbitals are of π-bonding-type orbitals. In all cases, LUMO and LUMO+1 orbitals are π^*-antibonding-type orbitals. An electronic system with a larger HOMO–LUMO gap should be less reactive than the one having a smaller gap [45]. Therefore, the value of energy separation between the HOMO and LUMO orbitals is 5.539 eV, and this large energy gap indicates that the title structure is stable.

Nonlinear optical effects

The NLO effects arise from the interactions of electromagnetic fields in various media to produce new fields altered in phase, frequency, amplitude, or other propagation characteristics from incident fields [46]. NLO is at the forefront of current research because of its importance in providing the key functions of frequency shifting, optical modulation, optical switching, optical logic, and optical memory for emerging technologies in the areas such as telecommunications, signal processing, and optical interconnections [47–50].

The nonlinear optical response of an isolated molecule in an electric field $E_i(\omega)$ can be presented as a Taylor series expansion of the total dipole moment, μ_{tot}, induced by the field:

$$\mu_{\text{tot}} = \mu_o + \alpha_{ij}E_j + \beta_{ijk}E_jE_k + \ldots, \tag{2}$$

where α_{ij} is the linear polarizability, μ_o is the permanent dipole moment, and β_{ijk} are the first hyperpolarizability tensor components. The isotropic (or average) linear polarizability is defined as [51] follows:

$$\alpha_{\text{tot}} = \frac{\alpha_{xx} + \alpha_{yy} + \alpha_{zz}}{3}. \tag{3}$$

The first hyperpolarizability is a third rank tensor that can be described by $3 \times 3 \times 3$ matrix. The 27 components of 3D matrix can be reduced to 10 components due to the Kleinman symmetry [52] $\left(\beta_{xyy} = \beta_{yxy} = \beta_{yyx},\ \beta_{yyz} = \beta_{yzy} = \beta_{zyy}; \ldots\right.$ likewise other permutations also take

Table 6. HOMO–LUMO gap, total dipole moment (μ), polarizability (α), and the first hyperpolarizability (β) of the title compound.

Basis set	μ (Debye)	α (Å^3)	β (cm^5/esu) $\times 10^{-30}$
6-31G(d)	1.535	31.301	1.270
6-31++G(d, p)	1.293	36.415	0.512
6-311++G(d, p)	1.277	36.523	0.536

the same value). The output from Gaussian 03 provides 10 components of this matrix as β_{xxx}, β_{xxy}, β_{xyy}, β_{yyy}, β_{xxz}, β_{xyz}, β_{yyz}, β_{xzz}, β_{yzz}, β_{zzz}. The components of the first hyperpolarizability can be calculated using the following equation [51]:

$$\beta_i = \beta_{iii} + \frac{1}{3}\sum_{i\neq j}\left(\beta_{ijj} + \beta_{jij} + \beta_{jji}\right). \tag{4}$$

Using the x, y, and z components of β, the magnitude of the first hyperpolarizability tensor can be calculated as follows:

$$\beta_{\text{tot}} = \sqrt{(\beta_x^2 + \beta_y^2 + \beta_z^2)}. \tag{5}$$

The complete equation for calculating the magnitude of β from Gaussian 03W output is given as follows:

$$\beta_{\text{tot}} = \sqrt{(\beta_{xxx} + \beta_{xyy} + \beta_{xzz})^2 + (\beta_{yyy} + \beta_{yzz} + \beta_{yxx})^2 + (\beta_{zzz} + \beta_{zxx} + \beta_{zyy})^2}. \tag{6}$$

The calculations of the total molecular dipole moment (μ), linear polarizability (α), and the first-order hyperpolarizability (β) from the Gaussian output have been explained in detail previously [52], and DFT has been extensively used as an effective method to investigate the organic NLO materials [53–58]. To investigate the effects of basis sets on the NLO properties of the compound I, the μ_{tot}, α_{tot}, and β_{tot} were calculated by the B3LYP method with 6-31G(d), 6-31++G(d, p), and 6-311++G(d, p) basis sets, as listed in Table 6.

We see in Table 6 that calculated values of μ_{tot}, α_{tot}, and β_{tot} slightly depend on the size of basis sets. Obtained value of the μ_{tot} with 6-31G(d) basis set is bigger than those obtained with larger size of basis sets. However, the α_{tot} value obtained by the small size of basis set is smaller than that of large size of basis set. Besides, obtained value of β_{tot} with 6-31G(d) basis set is bigger than other large basis sets.

Urea is one of the prototypical molecules used in the study of the NLO properties of molecular systems. Therefore, it was frequently used as a threshold value for comparative purposes. It can be seen in Table 6 that the calculated values of α_{tot} and β_{tot} for the title molecule are greater than those of urea (α_{tot} and β_{tot} for urea are 3.831 Å^3 and 0.3728×10^{-30} cm^5/esu respectively obtained by the B3LYP/6-31G(d) method). These results indicate that the title compound may be a potential candidate of the second-order NLO material.

Conclusions

In this work, the title compound has been characterized by ^{1}H-, ^{13}C-NMR, X-ray analysis, and FT-IR techniques. Crystal structure is stabilized by the O–H···N hydrogen bond interactions. To support the solid state structure, the geometric parameters, vibrational frequencies, and ^{1}H- and ^{13}C-NMR chemical shifts of the title compound have been calculated using the DFT/B3LYP method with the 6-31G(d) basis set, and compared with experimental findings. The calculated results show that the optimized geometries can well reproduce the crystal

structure, and the theoretical vibrational frequencies and chemical shift values. The MEP map shows that the negative potential sites are on electronegative nitrogen atom, while the positive potential site is around the oxygen atom. These sites give information about the region from where the compound can undergo intra- and intermolecular interactions. The predicted NLO properties of the title compound are greater than those of urea. The title compound may be a candidate as a second-order nonlinear optical material. As a result, all of these calculations will provide helpful information for further studies on the title compound.

References

[1] Marquis, R., Sheng, J., Nguyen, T., Baldeck, J., & Olsson, J. (2006). *Arch. Oral Biol.*, *51*, 1015.
[2] Mavrova, A. Ts. (2006). *J. Eur. Med. Chem.*, *41*, 1412.
[3] Cheng, J., Jiangtao, X., & Xianjin, L. (2005). *Bioorg. Med. Chem. Lett.*, *17*, 267.
[4] Nakashima, K., Yamasaki, H., Kuroda, N., & Akiyama, S. (1995). *Anal. Chim. Acta*, *303*, 103.
[5] Nakashima, K. (2003). *Biomed. Chromatogr.*, *17*, 83.
[6] Lipshutz, B. H. (1986). *Chem. Rev.*, *86*, 795.
[7] Al-Soud, Y. A., Al-Masoudi, N. A., Hassan, H. G., Clercq, E. D., & Pannecouque, C. (2007). *Acta Pharm.*, *57*, 379.
[8] Kelley, J. L., Thompson, J. B., Styles, V. L., Soroko, F. E., & Cooper, B. R. (1995). *J. Heterocycl. Chem.*, *32*, 1423.
[9] Gadad, A. K., Noolvi, M. N., & Karpoormath, R. V. (2004). *Bioorg. Med. Chem.*, *12*, 5651.
[10] Wan, S. B., Chu, F. M., & Guo, Z. R. (2002). *Acta Pamaceut. Sin.*, *37*, 516 (in Chinese).
[11] Laufer, S., & Koch, P. (2008). *Biomol. Chem.*, *6*, 437.
[12] Celik, A., & Aras Ates, N. (2006). *Drug Chem. Toxicol.*, *29*, 85.
[13] Adams, G. E., & Stratford, I. J. (1994). *Int. J. Radiat. Oncol. Biol. Phys.*, *29*, 231.
[14] Kapoor, V. K., Chadha, R., Venisetty, P. K., & Prasanth, S. (2003). *J. Sci. Ind. Res.*, *62*, 659 (India).
[15] Wheate, N. J., Walker, S., Craig, G. E., & Oun, R. (2010). *Dalton Trans.*, *39*, 8113.
[16] Ashani, Y., Radic, Z., Tsigelny, I., Vellom, D. C., Pickering, N. A., et al. (1995). *J. Biol. Chem.*, *270*, 6370.
[17] Sheldrick, G. M. (1997). *SHELXS-97 and SHELXL-97*, University of Gottingen: Gottingen, Germany.
[18] Ellingson, B. A., Theis, D. P., Tishchenko, O., Zheng, J., & Truhlar, D. G. (2007). *J. Phys. Chem. A*, *111*, 13554.
[19] Ditchfield, R. (1972). *J. Chem. Phys.*, *56*, 5688.
[20] Wolinski, K., Hinton, J. F., & Pulay, P. (1990). *J. Am. Chem. Soc.*, *112*, 8251.
[21] Dennington, R. I. I., Keith, T., & Millam, J. (2007). *GaussView, Version 4.1.2*, Semichem: Shawnee Mission, KS.
[22] Frisch, M. J., Trucks, G. W., Schlegel, H. B., Scuseria, G. E., Robb, M. A., et al. (2004). *Gaussian 03, Revision E.01*. Gaussian: Wallingford, CT.
[23] Politzer, P., & Murray, J. S. (2002). *Theor. Chem. Acc.*, *108*, 134.
[24] Soylu, M. S., Yüksektepe, Ç., Çalışkan, N., Özel, S., & Servi, S. (2011). *J. Chem. Crystallogr.*, *41*, 1968.
[25] Tanak H., Köysal, Y., Ünver, Y., Yavuz, M., Işık, Ş., and Sancak, K. (2010). *Mol. Phys.*, *108*(*2*), 127.
[26] Yüksektepe, Ç., Saraçoğlu, H., Çalışkan, N., A, & Cukurovali, A. (2010). *Mol. Cryst. Liq. Cryst.*, *533*, 126.
[27] Yüksektepe, Ç., Soylu, M. S., Saraçoğlu, H., Yılmaz, İ., Cukurovali, A., and Çalışkan, N. et al. (2005). *Acta Cryst.*, *E61*, O1158.
[28] Yüksektepe, Ç., Soylu, M. S., Saraçoğlu, H., Çalışkan, N., Cukurovali, A., et al. (2005). *Acta Cryst.*, *E61*, O2384.
[29] Yüksektepe, Ç., Saraçoğlu, H., Çalışkan, N., Yılmaz, İ., & Cukurovali, A. (2010). *Bull. Korean Chem. Soc.*, *31*(*12*), 3553.
[30] Bernstein, J., Davis, R. E., Shimoni, L., & Chang, N.-L. (1995). *Angew. Chem. Int. Ed. Engl.*, *34*, 1555.
[31] Kowalczyk, I., Bartoszak-Adamska, E., Jasko´ Lski, M., Dega-Szafran, Z., & Szafran, M. (2010). *J. Mol. Struc.*, *976*, 119.

[32] Smith, B., (1999). *Infrared Spectral Interpretation, a Systematic Approach*, CRC Press: Washington, DC.
[33] Silverstein, R. M., & Webster, F. X. (2003). *Spectroscopic Identification of Organic Compounds, Sixth ed.*, John Wiley: New York, NY.
[34] Teimouri, A., Emami, M., Chermahini, A. N., & Dabbagh, H. A. (2009). *Spectrochim. Acta*, *71A*, 1749.
[35] Sajan, D., Binoy, J., Pradeep, B., Krishnan, K. V., Kartha, V. B., et al. (2004). *Spectrochim. Acta*, *60A*, 173.
[36] Furic, K., Mohack, V., Bonifacic, M., & Stefanic, I. (1992). *J. Mol. Struct.*, *267*, 39.
[37] Scrocco, E., & Tomasi, J. (1978). *Adv. Quant. Chem.*, *11*, 115.
[38] Luque, F. J., Lopez, J. M., & Orozco, M. (2000). *Theor. Chem. Acc.*, *103*, 343.
[39] Okulik, N., & Jubert, A. H. (2005). *Internet Electron J. Mol. Des.*, *4*, 17.
[40] Politzer, P., Laurence, P. R., & Jayasuriya, K. (1985). *Environ. Health Perspect.*, *61*, 191.
[41] Scrocco, E., & Tomasi, J. (1973). *Topics Current Chem.*, *7*, 95.
[42] Politzer, P., & Truhlar, D. G., (1981). *Chemical Applications of Atomic and Molecular Electrostatic Potentials*, Plenum Press: New York, NY.
[43] Politzer, P., Concha, M. C., & Murray, J. S. (2000). *Int. J. Quantum Chem.*, *80*, 184.
[44] Fleming, I. (1976). *Frontier Orbitals and Organic Chemical Reactions*, John Wiley: London.
[45] Kurtaran, R., Odabaşoğlu, S., Azizoğlu, A., Kara, H., & Atakol, O. (2007). *Polyhedron*, *26*, 5069.
[46] Sun, Y. X., Hao, Q. L., Wei, W. X., Yu, Z. X., Lu, L. D., et al. (2009). *J. Mol. Struct. Theochem.*, *904*, 74.
[47] Andraud, C., Brotin, T., Garcia, C., Pelle, F., Goldner, P., et al. (1994). *J. Am. Chem. Soc.*, *116*, 2094.
[48] Geskin, V. M., Lambert, C., & Bredas, J. L. (2003). *J. Am. Chem. Soc.*, *125*, 15651.
[49] Nakano, M., Fujita, H., Takahata, M., & Yamaguchi, K. (2002). *J. Am. Chem. Soc.*, *124*, 9648.
[50] Sajan, D., Joe, H., Jayakumar, V. S., & Zaleski, J. (2006). *J. Mol. Struct.*, *785*, 43.
[51] Zhang, R., Du, B., Sun, G., & Sun, Y. X. (2010). *Spectrochim. Acta*, *75A*, 1115.
[52] Kleinman, D. A. (1962). *Phys. Rev.*, *126*, 1977.
[53] Thanthiriwatte, K. S., & Nalin de Silva, K. M. (2002). *THEOCHEM. J. Mol. Struct.*, *617*, 169.
[54] Sun, Y. X., Hao, Q. L., Yu, Z. X., Wei, W. X., Lu, L. D., & Wang, X. (2009). *Mol. Phys.*, *107*, 223.
[55] Ahmed, A. B., Feki, H., Abid, Y., Boughzala, H., Minot, C., & Mlayah, A. (2009). *J. Mol. Struct.*, *920*, 1.
[56] Abraham, J. P., Sajan, D., Shettigar, V., Dharmaprakash, S. M., Nemec, I., et al. (2009). *J. Mol. Struct.*, *917*, 27.
[57] Sagdinc, S. G., & Esme, A. (2010). *Spectrochim. Acta*, *75A*, 1370.
[58] Ahmed, A. B., Feki, H., Abid, Y., Boughzala, H., & Minot, C. (2010). *Spectrochim. Acta*, *75A*, 293.